A Minimal Transmembrane β-Barrel Platform Protein Studied by Nuclear Magnetic Resonance[†,‡]

Maria U. Johansson,[*,§,||,⊥] Simon Alioth,[§,⊥] Kaifeng Hu,[§,@] Reto Walser,[§,#] Ralf Koebnik,[+] and Konstantin Pervushin[*,§]

Laboratorium für Physikalische Chemie, ETH Hönggerberg, Wolfgang-Pauli-Strasse 10, CH-8093 Zürich, Switzerland, and Institut für Genetik, Martin-Luther-Universität Halle-Wittenberg, Weinbergweg 10, D-06120 Halle (Saale), Germany

Received June 24, 2006; Revised Manuscript Received November 21, 2006

ABSTRACT: In this study, we were concerned with the structural role of the surface-exposed extracellular loops of the N-terminal transmembrane (TM) domain of OmpA. A variant of the TM domain of outer membrane protein A (OmpA) with all four such loops shortened, which we call the β-barrel platform (BBP), was successfully refolded. This indicates that the removed parts of the surface-exposed loops indeed do not contain amino acid sequences critical for this membrane protein's refolding in vitro. BBP has the potential to be used as a template β-barrel membrane protein structure for the development of novel functions, although our results also highlight the potential difficulties that can arise when functionality is being engineered into the loop regions of membrane proteins. We have used solution nuclear magnetic resonance spectroscopy to determine the global fold of BBP+EF, BBP with a metal ion-binding EF-hand inserted in one of the shortened loops. BBP and BBP+EF in dihexanoylphosphatidylcholine micelles are eight-stranded antiparallel β-barrels, and BBP represents the smallest β-structured integral membrane protein known to date.

Outer membrane protein A (OmpA)[1] is one of the major outer membrane proteins of *Escherichia coli* (for a review, see ref *1*). OmpA is composed of two domains: an N-terminal transmembrane (TM) domain and a C-terminal periplasmic domain (*2*). The three-dimensional (3D) structure of the TM domain has been determined by X-ray crystallography (*3*, *4*) as well as by nuclear magnetic resonance (NMR) spectroscopy (*5*). This domain is composed of eight antiparallel β-strands connected by four relatively large surface-exposed extracellular loops and three short periplasmic turns which form a β-barrel.

To study the structural and functional roles of the surface-exposed loops of the N-terminal TM domain of OmpA, they were shortened separately and in all possible combinations in an earlier study (for details, see ref *6* and references therein). The smallest variant among these has all four surface-exposed loops shortened and is termed OmpAΔL1234. If, like the TM domain of OmpA, this variant adopts a β-barrel structure, it would be the smallest β-structured integral membrane protein known to date, and this is, in fact, one of the reasons for our choice of OmpAΔL1234 as the model protein for the development of new NMR methods for studies of membrane proteins in solution. The plasmid holding the gene for OmpAΔL1234 was constructed in such a way that each shortened surface loop contains unique and compatible restriction endonuclease recognition sites in the same reading frame (*6*). In principle, this arrangement of the restriction sites allows the insertion of arbitrary sequences of amino acids, although it should be noted that, in reality, the ability of the TM domain of OmpA to accept foreign sequences can be limited (*7*). The possibility of inserting a

[†] This work was supported by a Swiss National Fund grant (to K.P.), by an ETH internal grant (to K.P.), and by the Swedish Foundation for International Cooperation in Research and Higher Education (STINT) in the form of a postdoctoral fellowship (to M.U.J.).

[‡] The coordinates of the 10 lowest-energy structures and the NMR data of BBP+EF have been deposited with the RCSB Protein Data Bank and BMRB as entries 2jmm and 15045, respectively.

* To whom correspondence should be addressed. M.U.J.: e-mail, maria.johansson@nmr.gu.se; telephone, +46 31 7733884; fax, +46 31 7733880. K.P.: e-mail, konstantin.pervushin@bionmr.phys.chem.ethz.ch; telephone, +41 44 6320922; fax, +41 44 6321021.

[§] ETH Hönggerberg.

[||] Present address: The Hasselblad Laboratory, The Swedish NMR Centre at Göteborg University, Medicinaregatan 5C, SE-413 90 Göteborg, Sweden.

[⊥] These authors contributed equally to this work.

[@] Present address: Laboratory of Chemical Physics, National Institute of Diabetes and Digestive and Kidney Diseases, National Institutes of Health, Bethesda, MD 20892-0520.

[#] Present address: Institute of Organic Chemistry, University of Zurich, Winterthurerstrasse 190, CH-8057 Zurich, Switzerland.

[+] Martin-Luther-Universität Halle-Wittenberg.

[1] Abbreviations: 2D and 3D, two- and three-dimensional, respectively; BBP, β-barrel platform; BBP+EF, BBP with an EF-hand loop inserted in the third shortened surface-exposed extracellular loop; BBP+EF+2G, BBP+EF with two flanking Gly residues; β-OG, *n*-octyl D-glucoside; cmc, critical micelle concentration; CSI, chemical shift index; DHPC, dihexanoylphosphatidylcholine (1,2-dihexanoyl-*sn*-glycero-3-phosphocholine); DPC, dodecylphosphocholine; DSS, 2,2-dimethyl-2-silapentane-5-sulfonate sodium salt; Gdn-HCl, guanidine hydrochloride; HSQC, heteronuclear single-quantum coherence; IPTG, isopropyl β-D-thiogalactopyranoside; MALDI, matrix-assisted laser desorption ionization; NMR, nuclear magnetic resonance; NOE, nuclear Overhauser enhancement; NOESY, NOE spectroscopy; octyl-POE, *n*-octyl polyoxyethylene; OmpA, outer membrane protein A; PDB, Protein Data Bank; R_1, longitudinal relaxation rate constant; R_2, transverse relaxation rate constant; RDC, residual dipolar coupling; rmsd, root-mean-square deviation; TE buffer, 20 mM Tris-HCl and 5 mM EDTA; TM, transmembrane; TROSY, transverse relaxation-optimized spectroscopy.

10.1021/bi061265e CCC: $37.00 © 2007 American Chemical Society
Published on Web 01/09/2007

variety of different loop structures into the shortened surface-exposed loops of OmpAΔL1234 in combination with its small size has led us to refer to it as the β-barrel platform (BBP).[2]

The motivation for the NMR studies of BBP described in this paper is to see if BBP indeed does adopt a β-barrel structure very similar to the wild-type protein and if the removed parts of the loops contain amino acid sequences that are critical for the folding of this integral membrane protein in vitro. In addition, we expect that BBP may be useful as a TM β-barrel scaffold onto which different functionalities can relatively easily be grafted. The resulting artificial integral membrane proteins may have several interesting applications (for a review, see ref *8*). Finally, we believe that BBP is an excellent model protein for the development of new NMR methods for studies of membrane proteins in solution.

Membrane proteins are difficult to study by NMR because of their slow rotation in solution, resulting in broad lines in the spectrum. Of the 111 unique entries in the database[3] of membrane proteins of known 3D structure (maintained by S. White at the University of California, Irvine, CA), only four entries are the result of NMR investigations. Three of these are β-barrel membrane proteins (*5*, *9*, *10*), and one is a four-helix bundle membrane-integrating protein (*11*). In addition to suffering from broad lines, the chemical shift dispersion is generally limited for membrane proteins due to exclusively α-helical or β-stranded secondary structure. Even in cases when it is possible to obtain backbone assignments from uniformly ^{2}H-, ^{13}C-, and ^{15}N-labeled proteins, this labeling makes it effectively impossible to obtain enough long-range nuclear Overhauser effects (NOEs) to determine the tertiary fold of the protein to high precision (*5*, *9*, *10*), as will be further exemplified in this study. Consequently, membrane proteins reconstituted into micelles (e.g., BBP) and other large complexes (with deuterated amino acid side chains) call for complementary techniques of structure determination by NMR, which preferably do not rely on the conventionally used NOE effect.

Measurement of residual dipolar couplings (RDCs) has already established itself as a significant auxiliary source of structural constraints (for a review, see ref *12*). To enable measurement of RDCs, weak alignment in the samples has to be induced. Unfortunately, hydrophobic membrane proteins and their associated lipids interact with and disrupt the most commonly employed orienting agents, including bicelles (*13*), filamentous bacteriophages (*14*, *15*), and purple membrane fragments (*16*, *17*). However, the binding of lanthanides to metal ion binding motifs in proteins also has the potential to weakly align proteins in strong magnetic fields (*18*), but one cannot rely on the proteins under study to contain natural metal ion binding motifs to be exploited for saturation with lanthanide ions (*19*). A complementary strategy would therefore be to introduce such a metal ion binding motif using standard microbiology techniques (*20*). Such a construct is depicted in Figure 1B. Another strategy which has recently been used with success is alignment in polyacrylamide gels (*21*, *22*).

Therefore, after successfully having refolded BBP, we decided to insert a 12-amino acid sequence corresponding to loop III of calmodulin from *Xenopus laevis*, i.e., a so-called EF-hand loop, into BBP (the resulting construct will henceforth be denoted BBP+EF). As in similar studies (*23*, *24*), this insert had to be subsequently adjusted to endow some structural flexibility to facilitate higher-affinity metal ion binding. In its natural context, this loop strongly binds to calcium (*25*), and it has been shown that in calmodulin, calcium can be replaced with lanthanides (*26*). The values for binding of terbium (Tb^{3+}) and lanthanum (La^{3+}) to loop III of calmodulin have been shown to be 20 ± 6 and 40 ± 7 μM, respectively (*27*). Insertion of lanthanide binding sites, such as in BBP+EF, can be used as a general method for achieving alignment to enable measurement of RDCs and thereby obtain higher-resolution NMR structures of membrane proteins. An EF-hand loop has previously been added to the N-terminus of Vpu, an 81-residue membrane-associated protein, for the purpose of measuring RDCs (*20*), but to our knowledge, EF-hand loops have not previously been inserted into an integral membrane protein.

MATERIALS AND METHODS

Construction of the BBP Gene. To produce the BBP protein at a high level intracellularly in the form of inclusion bodies, a variant of the *ompA*ΔL1234 gene was constructed without the region encoding the signal peptide for secretion (*6*). Upon a polymerase chain reaction (PCR) using the *ompA*ΔL1234 plasmid (*6*) as template DNA and two primers containing an *Nde*I and a *Bam*HI restriction site (forward primer, 5′-GGCATCCCAT ATG CCG AAA GAT AAC ACC TGG TAC ACT GGT GC; reverse primer, 5′-CGGGATCC TCA AGC TGC CTC GCC CTG ACC GAA ACG G), respectively, the product was cloned into pET-3b (Novagen) which was transformed into *E. coli* BL21-Gold-(DE3) (Strategene). The sequence was confirmed by DNA sequencing. A matrix-assisted laser desorption ionization (MALDI) mass spectrum of the expressed protein showed a molecular mass of 15 681 Da, which is within reasonable range of the theoretical average mass of 15 673.6 Da (with the N-terminal Met removed; see Figure 1A).

Engineering of a Metal Ion-Binding EF-Hand Loop to BBP. The calcium-binding EF-hand loop III from calmodulin (DKDGNGYISAAE) was amplified from a plasmid containing the calmodulin gene of *X. laevis*. The two primers used for PCR contained a *Spe*I and an *Nhe*I restriction site (forward primer, 5′-GG ACT AGT GAC AAG GAT GGC; reverse primer, 5′-CTA GCT AGC TTC AGC AGC ACT G). The amplified product was inserted into *ompA*ΔL1234 by means of the *Spe*I restriction site corresponding to the third shortened surface-exposed loop of the protein. The resulting BBP+EF construct contained 14 additional amino acids (DKDGNGYISAAEAS), 12 (underlined) from the EF-hand loop III of *X. laevis* calmodulin and two for the *Nhe*I−*Spe*I ligation (AS). The sequence was confirmed by DNA sequencing. Yet another construct, which we call BBP+EF+2G, was prepared in a similar way, but with an insert containing two flanking Gly residues (i.e., **G**DKDGNGYISAAE**G**AS) to improve Tb^{3+} affinity.

[2] BBP contains five additional residues in the C-terminus, and the starting residues are Pro and Lys instead of Ala, Pro, and Lys (as in the OmpAΔL1234 construct).

[3] http://blanco.biomol.uci.edu/Membrane_Proteins_xtal.html, updated June 8, 2006.

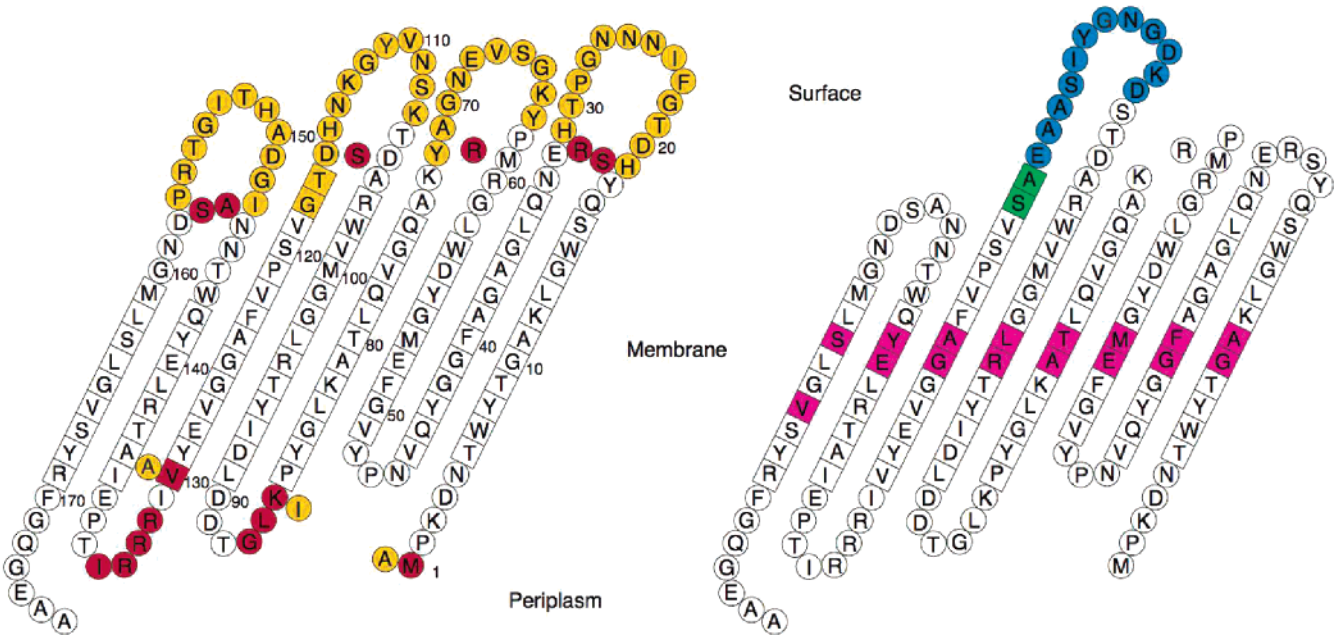

FIGURE 1: Schematic models of variants of TM OmpA domains. All β-barrel residues [as defined by the NMR structure of the TM domain of OmpA (*5*)] are represented by squares. The numbering of amino acid residues follows that of the TM domain of OmpA (*5*) throughout the paper (except in Figure 5). (A) BBP is a mutant of the TM domain of OmpA. Residues that are present in the wild-type TM domain of OmpA (but not in BBP) are colored yellow, whereas residues that are present in BBP (but not in the TM domain of OmpA) are colored red. In essence, the four surface-exposed extracellular loops of the TM domain of OmpA (colored yellow) have been replaced with Ser-Arg, Arg, Ser, and Ala-Ser (colored red) residues in BBP. There are also slight modifications in two periplasmic turns. Ile87 (yellow) in the second turn is replaced with a Lys-Leu-Gly sequence (red), and the Arg-Arg-Arg-Ile peptide (red) is inserted between Ile131 and Thr132 in the third turn. In addition, the Ala (yellow) at position 130 is changed to a Val (red). Finally, the N-terminal amino acid sequence in the TM domain of OmpA is Ala-Pro-Lys, but in the clone, we used in this study, the N-terminal sequence is (Met)-Pro-Lys. Finally, an extra Gln-Gly-Glu-Ala-Ala sequence is present at the C-terminus (but not in the original OmpAΔL1234 construct). (B) BBP+EF is the same as BBP described in panel A except that a 12-amino acid residue segment (colored blue) corresponding to loop III of calmodulin from *X. laevis* (i.e., a so-called EF-hand loop) has been inserted into BBP and two residues, Ala and Ser (colored green), were added for the *Nhe*I−*Spe*I ligation. The meaning of the purple coloring is explained in the legend of Figure 6.

Overexpression and Isolation from Inclusion Bodies. The plasmid holding the gene of interest was transformed into *E. coli* BL21-Gold(DE3)pLysS competent cells (Stratagene). The freshly transformed cells were grown in LB medium overnight. This culture was inoculated into M9 minimal medium (1:100) with ^{15}N-labeled ammonium chloride (1 g/L, >99% ^{15}N) and glucose (2 g/L, >98% $^{13}C_6$-D-labeled in some cases). In addition, the medium contained 10% correspondingly labeled Celtone complete medium as well as vitamins and trace elements. All isotopically labeled compounds were from Spectra Stable Isotopes. For preparation of deuterated samples, 99% ^2H_2O was used as the solvent instead of H_2O with a two-step adaptation of the growing cultures in 50% $^2H_2O/H_2O$ LB medium and 100% ^2H_2O LB medium. All cultures were grown at 37 °C and contained 100 μg/mL ampicillin and 10 μg/mL chloramphenicol. Protein expression was induced with 1 mM isopropyl β-D-thiogalactopyranoside (IPTG) at an OD_{600} of 0.3−0.4, and cells were harvested by centrifugation when cell growth reached its stationary phase. The protein was expressed in inclusion bodies. The pellet was frozen, then thawed on ice, and resuspended in 20 mM Tris-HCl and 5 mM EDTA (TE buffer) (pH 8) with a volume (in mL) corresponding to 3 times the wet weight (in grams) of the pellet. To lyse the cells, the resuspended pellet was sonicated for 20−30 min on crushed ice and then centrifuged for 1 h at 4300*g* and 4 °C. The white inclusion body pellet was collected and resuspended in TE buffer (pH 8) containing 2% Triton X-100 with a volume (in milliliters) again corresponding to ~3 times the wet weight (in grams) of the pellet, shaken at 37 °C for 20 min, and thereafter centrifuged for 30 min at 4300*g* and 4 °C. The pellet was resuspended in 30 mL of TE buffer (pH 8), shaken for 1 h at 37 °C, and then centrifuged for 30 min at 4300*g* and 4 °C. The pellet was resuspended in a minimal amount of 6 M guanidine hydrochloride (Gdn-HCl) in TE buffer (pH 6), shaken for at least 2 h at 37 °C, and centrifuged for 20 min at 47800*g* and 4 °C, and the supernatant was collected. The purity was checked using SDS−PAGE. For specific ^{15}N labeling, the plasmid containing BBP+EF was transformed into the transaminase knockout strain *E. coli* D39(DE3). The protein was expressed in unlabeled medium (vide supra) containing 75 mg/L ^{15}N-labeled Leu (>98% ^{15}N, Spectra Stable Isotopes). The labeled amino acid was added immediately prior to the induction (*28*).

Refolding of BBP. Refolding of BBP required screening of a large space of refolding conditions, and therefore, a fractional factorial approach (*29*) was used to identify suitable refolding conditions for BBP. In brief, eight factors with two levels for each factor were combined into a 16-condition fractional factorial screen (*30*, *31*). We considered the following eight factors: pH (MES at pH 6 or HEPES at pH 7), detergent [*n*-octyl polyoxyethylene (octyl-POE) (Bachem) or dihexanoylphosphatidylcholine (DHPC) (Avanti Polar Lipids)], and the presence or absence of divalent cations, glycerol, Gdn-HCl, nondetergent sulfobetaine (*32*), L-arginine, and ammonium sulfate. The protein sample to be refolded was diluted to 0.4 mM (estimated by the absorbance

at 278 nm) in 6 M Gdn-HCl and TE buffer (pH 6). One volume of the denatured protein solution was slowly diluted into 7 volumes of the refolding buffer at room temperature while the mixture was stirred vigorously, resulting in 8 volumes of the following solution: 0.1 M MES buffer (pH 6) in the presence of 2.4% (~53 mM) DHPC [critical micelle concentration (cmc) = 14 mM (*33*)], 1.0 M Gdn-HCl, 0.5 M ammonium sulfate, 0.4 M glycerol, 0.35 M L-arginine, 0.1 M NaCl, and 5 mM EDTA. The solution was then stirred overnight, concentrated, and dialyzed four times against 1 L of 20 mM MES buffer (pH 6) and 0.02% sodium azide using a 3 mL Slide-A-Lyzer 3.5 kDa cutoff dialysis cassette (Pierce) at room temperature, and the level of DHPC was maintained at 2.4% by addition of detergent into the dialysis cassette. The protein sample was then concentrated to a volume of 400 μL (same buffer but including 5% ^2H_2O) and subsequently transferred to a NMR tube (Shigemi); 10 kDa centrifugal filter devices (Millipore) were used for all concentrations. For the refolding trials, uniformly ^{2}H- and ^{15}N-labeled BBP was used, and the outcomes of the trials were judged by the quality of obtained transverse relaxation-optimized spectroscopy (TROSY) spectra on a 600 MHz spectrometer equipped with a cryoprobe. A similar protocol was used for all BBP variants.

NMR Spectroscopy. NMR spectra, including two-dimensional (2D) ^{15}N$-^1$H (*34*) and 3D ^{15}N$-^1$H TROSY-HNCA (*35*) spectra, of BBP were acquired at 30 °C on a Bruker Avance 600 MHz spectrometer equipped with a cryogenic Z-gradient TXI probe. NMR spectra, including 2D ^{15}N$-^1$H TROSY and 3D ^{15}N$-^1$H TROSY-HNCA, 3D ^{15}N$-^1$H TROSY-HN(CO)CA (*36*), 3D ^{15}N$-^1$H TROSY-HNCO (*35*), 3D ^{15}N$-^1$H TROSY-HN(CA)CO (*36*), and 3D ^{15}N$-^1$H TROSY-HNCACB (*36*) spectra and one 3D ^{1}H$-^1$H NOESY-^{15}N$-^1$H HSQC (*37*) spectrum with a mixing time of 100 ms, of BBP+EF were acquired at 37 °C on the same 600 MHz spectrometer, and one 3D ^{1}H$-^1$H NOESY-^{15}N$-^1$H HSQC (as a sum of two spectra with mixing times of 80 and 160 ms, respectively) spectrum was acquired using a Bruker Avance 900 MHz spectrometer equipped with a cryogenic Z-gradient TXI probe at 37 °C. The sizes of the NMR spectra were typically 1024 complex points in the direct ^{1}H dimension and 40−80 and 40−128 complex points in the ^{13}C and ^{15}N dimensions, respectively. All 3D spectra were recorded with eight scans. Relaxation experiments with BBP+EF were conducted at 37 °C on the 600 MHz Bruker spectrometer using standard TROSY-based pulse sequences (*38*). The relaxation delays were 20, 70, 150, 300, 500, 900, 1100, 1500, 1700, and 2000 ms for the longitudinal relaxation rate constant (R_1) measurements and 0.5, 2, 5, 8, 11, 14, 16, 18, 22, 30, 50, and 70 ms for transverse relaxation rate constant (R_2) measurements. Estimates of R_1 and R_2 were determined by nonlinear least-squares fitting of two-parameter monoexponential functions to the measured peak intensities. The steady state ^{1}H$-^{15}$N NOE values were determined from the ratio of two different types of spectra, one with proton presaturation for 3 s and one without proton presaturation. Measurements of the lanthanide affinity of BBP+EF (1 mM) and BBP+EF+2G (0.6 mM) were performed by titration, using solutions of 0.5, 1.5, 3, and 5 mM $TbCl_3$ while recording 2D ^{15}N$-^1$H TROSY spectra at 37 °C on the 900 MHz Bruker spectrometer. RDCs were determined from TROSY and ^{15}N-anti-TROSY spectra, measured with and without Tb^{3+}, recorded with 1024 points in the direct ^{1}H dimension and 300 points in the indirect ^{15}N dimension with 64 scans at 900 MHz, using the TROSY and anti-TROSY component (ST2-PT elements) along the nitrogen dimension (*39*). The coupling was assessed in the indirect nitrogen dimension, because the line width in the proton dimension was more affected by the paramagnetic ions. NMR data were processed using either PROSA (*40*) or XWIN-NMR (Bruker) and analyzed using CARA (*41*, *42*). The ^{1}H chemical shifts were referenced to 2,2-dimethyl-2-silapentane-5-sulfonate sodium salt (DSS) (*43*). The ^{13}C and ^{15}N chemical shifts were referenced indirectly using the ^{13}C/^{1}H and ^{15}N/^{1}H gyromagnetic ratios (*44*).

Collection of Conformational Restraints. Conformational constrains were obtained from a 3D ^{15}N-resolved ^{1}H$-^1$H NOESY spectrum recorded at 900 MHz. Upper distance limits corresponding to characteristic long-range $^1H^N-^1H^N$ NOEs between β-strands were set to 3.6 Å (*45*). For all remaining types of NOEs, upper distance limits were conservatively set to 5 Å. Backbone torsion angle constraints (ϕ and φ) were obtained using TALOS (*46*) and the $^{13}C^\alpha$, $^{13}C^\beta$, $^{13}C'$, and ^{15}N chemical shifts when all 10 best matches agreed for a prediction. Prior to using TALOS, the chemical shifts of BBP+EF were adjusted to be referenced to TSP for the ^{13}C atoms and to liquid ammonia for the ^{15}N atoms. The chemical shifts of the $^{13}C^\alpha$, $^{13}C^\beta$, and ^{15}N atoms were also modified to account for deuterium isotope effects (*47*). To enable comparisons with other recently calculated structures of membrane proteins [and that of Tamm and co-workers (*5*) in particular], hydrogen bond restraints were added to those residues which were identified as being part of the β-barrel (see Results and Discussion). Each such hydrogen bond was represented by two distance upper limits; the N−O distance was restrained to be in the range of 2.7−3.0 Å, and the $^1H^N$−O distance was restrained to be in the range of 1.8−2.0 Å.

Global Fold Determination of BBP+EF. Structure calculations were performed with CYANA (*48*) (version 1.0). A total of 160 conformers were calculated with CYANA according to a protocol such that each random starting structure was subjected to 20 000 steps of torsion angle dynamics (4000 steps of heating followed by 16 000 steps of annealing) followed by 1000 steps of conjugate gradient minimization. As in other protocols for calculating structures of membrane proteins, a small but representative subset of calculated structures was selected and each structure in this subset was subjected to additional geometry refinement. In our case, the 20 structures having the lowest target function values were selected and subjected to 6000 steps of Polak−Ribière (*49*) conjugate gradient energy minimization in vacuo, using Gromacs version 3.3.1 (*50*, *51*) and the GROMOS96 43b1 force field (*52*). Finally, the 10 structures with the lowest energy were selected to represent the NMR-derived global fold of BBP+EF in DHPC micelles.

RESULTS AND DISCUSSION

Refolding of BBP. Following the detailed description in Materials and Methods, BBP was overexpressed in *E. coli*, isolated from inclusion bodies, and refolded into micelles. While overexpression in *E. coli* and isolation from inclusion bodies essentially followed standard procedures, the refolding

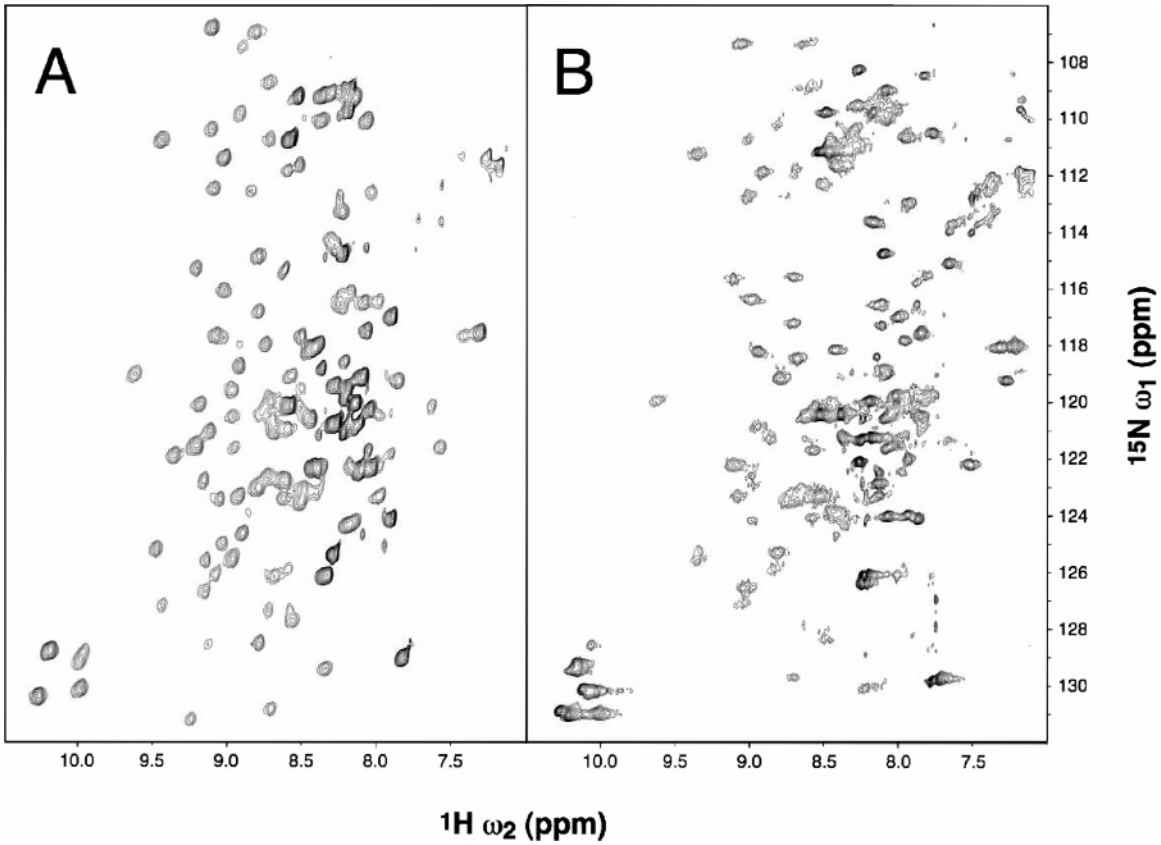

FIGURE 2: 2D $^{15}N-^{1}H$ TROSY spectrum of 1 mM uniformly ^{2}H-, ^{13}C-, and ^{15}N-labeled (A) BBP+EF and (B) BBP in DHPC micelles acquired at 600 MHz and 37 °C.

success was strongly dependent on the use of various additives and beneficial refolding procedures. Our initial attempts to refold BBP by directly using the previously published refolding protocol (*53*) resulted in solubilized but unfolded protein. Motivated by the need for a rapid and statistically meaningful method for evaluating and determining refolding conditions, we used a simplified version of a fractional factorial protein folding screen (*30*, *31*). The outcome of the refolding trials were judged by the quality of obtained TROSY spectra on a 600 MHz spectrometer equipped with a cryoprobe. Because the concentration of each sample was low, the use of a cryoprobe was essential for making judgments in reasonable time. By this, we have established conditions to refold BBP with an acceptable yield and such that peaks are well-dispersed in spectra (*34*). A 2D $^{15}N-^{1}H$ TROSY spectrum of ^{2}H-, ^{13}C-, and ^{15}N-labeled BBP in DHPC micelles at 37 °C, prepared as just described, is shown in Figure 2B and displays the large signal dispersion typical of a β-structured protein. This indicates that the removed parts of the surface-exposed loops indeed do not contain amino acid sequences critical for this membrane protein's refolding in vitro. Previously, it has been shown that the periplasmic turns also do not contain amino acid sequences that are critical for this protein's folding in vivo (*7*, *54*). Consequently, the fold, as described for the first time in this paper [previously only the topology of the protein in the outer membrane of *E. coli* in vivo was established (*6*) by comparative proteolytic digestion], adopted by this protein in vitro seems to be entirely determined by amino acid sequences in its TM regions. However, it is noteworthy that an influence of the periplasmic turns on the thermal stability of the OmpA TM domain (*6*) as well as on the efficiency of membrane assembly of circularly permuted variants of OmpA has been observed (*55*).

Engineering of a Metal Ion-Binding EF-Hand Loop to BBP. The successful refolding of BBP in vitro and the feasibility of preparing isotope-labeled samples suitable for NMR investigations encouraged us to engineer a metal ion-binding EF-hand loop into BBP to obtain an artificial membrane protein with a high affinity for paramagnetic ions, such as lanthanides. As discussed previously, binding of lanthanides to metal ion binding sites, such as EF-hand loops, has the potential to weakly align proteins in strong magnetic fields. This weak alignment may enable the measurement of RDCs and, thereby, provide additional structural constraints. The resulting BBP+EF construct contained 14 additional amino acids (DKDGNGYISAAEAS), 12 (underlined) from EF-hand loop III of *X. laevis* calmodulin and two for the *Nhe*I−*Spe*I ligation (AS). From 1 L of uniformly labeled (^{2}H, ^{13}C, and ^{15}N) medium, 400 μL of 1 mM BBP+EF could be obtained. The purity of the NMR sample was estimated to be approximately 95% as judged by SDS−PAGE. This sample was used for all measurements on BBP+EF. The 2D $^{15}N-^{1}H$ TROSY spectrum of uniformly ^{2}H, ^{13}C, and ^{15}N-labeled BBP+EF also displayed the large signal dispersion typical of a β-structured protein (Figure 2A) and thereby confirmed that the insertion of the EF-hand loop into the third shortened surface-exposed loop of BBP does not prevent BBP+EF from refolding in vitro in a manner similar to that of BBP, again demonstrating that the surface-exposed loops of the TM domain of OmpA are not required for proper folding. The spectra of BBP are consistently lower in quality than those of BBP+EF, as exemplified in Figure 2. We attribute this to enhanced

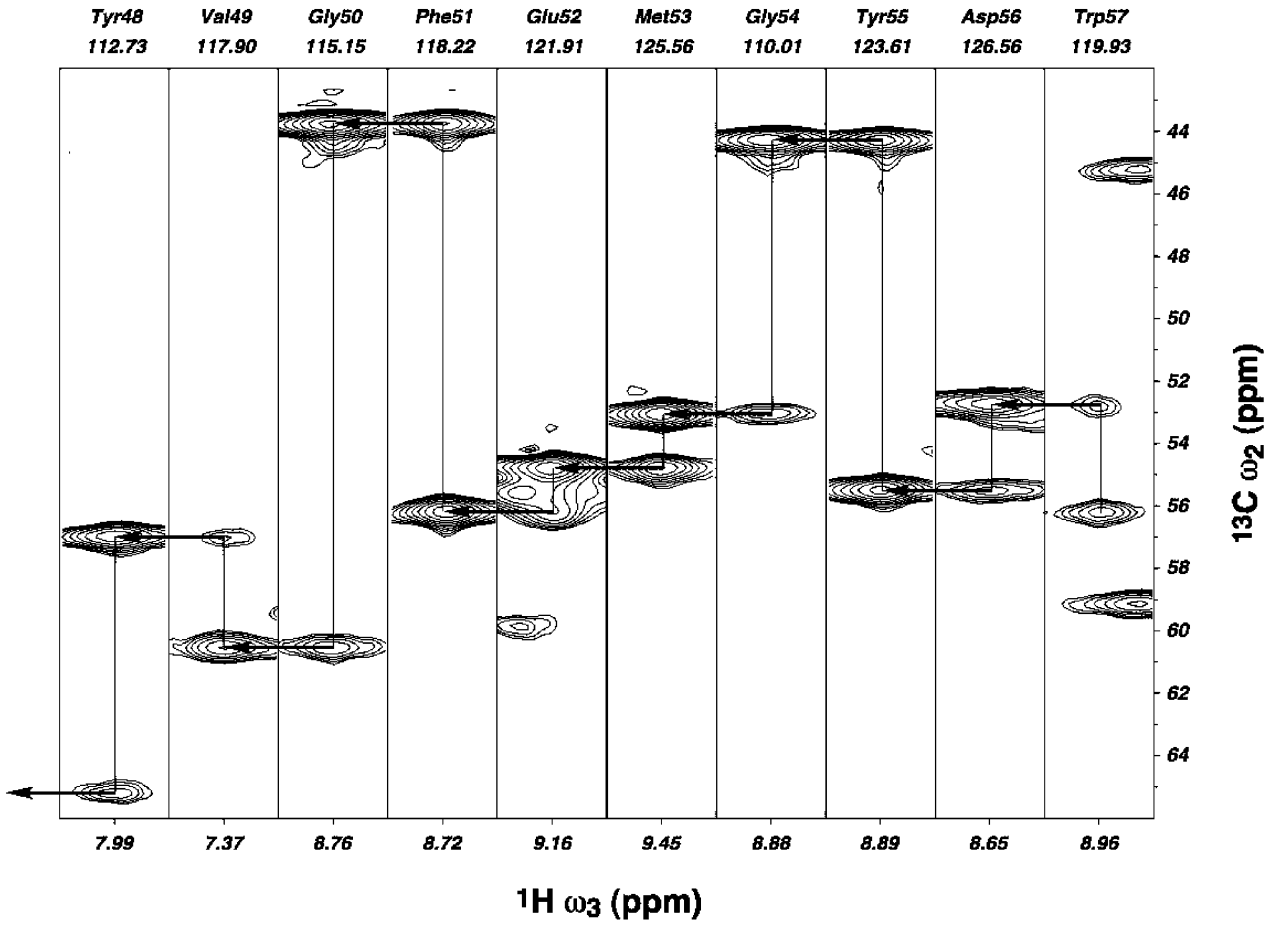

FIGURE 3: Strips from a 3D HNCA spectrum. The strips shown correspond to residues Tyr48−Trp57 in the third β-strand and were extracted from the spectrum at the ^{15}N chemical shifts of each residue (indicated at the top of the each strip together with the sequence specific assignment). Vertical lines connect the cross-peaks corresponding to the sequentially preceding and the intraresidual $^{13}C^{\alpha}$ of residue *i*, and the horizontal arrows point from the sequential $^{13}C^{\alpha}$ cross-peak of residue *i* to the intraresidual $^{13}C^{\alpha}$ cross-peak of residue $i - 1$. The spectrum was recorded at 600 MHz and 37 °C.

conformational exchange line broadening in BBP compared to BBP+EF. It may be that the insertion of the EF-hand loop into BBP releases structural tension possibly introduced by shortening the surface-exposed loops of the TM domain of OmpA.

Sequence Specific Backbone Assignment of BBP+EF. The sequence specific backbone assignment of BBP+EF was obtained by a combination of TROSY-type triple-resonance experiments: 3D ^{15}N−^{1}H TROSY-HNCA, 3D ^{15}N−^{1}H TROSY-HN(CO)CA, 3D ^{15}N−^{1}H TROSY-HNCO, 3D ^{15}N−^{1}H TROSY-HN(CA)CO, and 3D ^{15}N−^{1}H TROSY-HNCACB spectra of uniformly ^{2}H-, ^{13}C-, and ^{15}N-labeled BBP+EF. The assignment of Leu residues was corroborated by preparing a sample with only Leu residues labeled with ^{15}N.

Figure 3 shows strips from a 3D HNCA experiment corresponding to residues Tyr48−Trp57 in the third β-strand (Figure 1B). For all assigned residues, both the cross-peaks corresponding to the sequentially preceding and the intraresidual $^{13}C^{\alpha}$ could be identified (in the 3D HNCA spectrum) and distinguished between [in some cases using a 3D HN(CO)CA spectrum, which was of considerably lower quality]. For some residues, the cross-peak corresponding to the sequentially preceding $^{13}C^{\beta}$ is missing, but sequence specific assignment reliability was nonetheless possible to ensure by analysis of 3D HNCO and 3D HN(CA)CO spectra. Finally, when the sequence specific assignment was finished (residues 4−16, 27−46, 56−65, 70−84, 87−103, 106−115, 124−132, and 141−156 were assigned), the 3D ^{15}N-resolved ^{1}H−^{1}H NOESY spectrum was analyzed and, in addition to other purposes, served as a further validation of the sequence specific assignment.

The majority of the assigned residues are located in the TM β-strands. The residues residing in the shortened surface-exposed loops or in the slightly augmented (see Figure 1A for details) periplasmic turns have, for the most part, not been able to be assigned due to line broadening effects with the difficulties being relatively greater in the shortened surface-exposed loops. Similar assignment problems for the surface-exposed loops of the TM domain of OmpA were encountered in both dodecylphosphocholine (DPC) (*5*) and DHPC (*56*) micelles. In the case presented here, more than 70% of all residues were assigned, which is on par with the assignments of the TM domain of OmpA by the groups of Tamm (76%) (*5*) and Wüthrich (80%) (*56*). In both the mentioned studies of the TM domain of OmpA, the unassigned residues form a ring around the β-barrel between the core of the barrel and the surface-exposed extracellular loops. It has been argued that this may be because the corresponding peaks are broadened beyond detection due to conformational exchange processes. It has also been suggested that this phenomenon is a characteristic of the TM domain of OmpA, rather than the detergent, as similar behavior was seen for

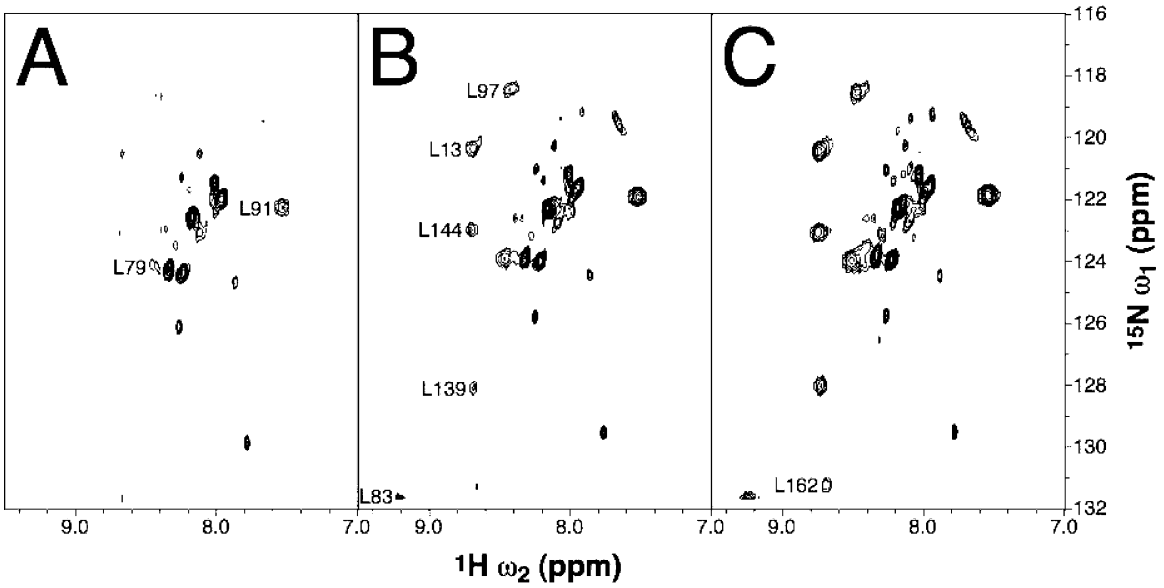

FIGURE 4: 2D ^{15}N−^{1}H TROSY spectra of a 0.3 mM Leu-selective ^{15}N-labeled BBP+EF sample, recorded at three different temperatures: (A) 30, (B) 37, and (C) 42 °C. The sequence specific assignments of the eight assigned leucines are given in the spectrum of the lowest temperature in which they are distinctly observed. The peaks in the middle are not assigned to the protein sequence and most probably stem from contaminating material or unfolded protein since their spectral intensity strongly depends on the sample preparation. The spectra were recorded at 600 MHz.

the TM domain of OmpA in both DPC and DHPC micelles. The effects of conformational exchange-induced line broadening strongly depend on the temperature at which measurements are conducted. At elevated temperatures, the exchange rates can be enhanced, resulting in detection of more and more of the expected Leu resonances in the specifically ^{15}N-labeled Leu sample (Figure 4).

It should be noted that sometimes the choice of detergent significantly affects which residues in the loop regions can be assigned. This is clearly illustrated by PagP in DPC micelles for which many residues in the extracellular surface-exposed loops are not assigned, whereas for PagP in *n*-octyl D-glucoside (β-OG) micelles, only two of these are not assigned. On the other hand, in β-OG micelles a few periplasmic residues are not assigned, which can be assigned in DPC micelles (*10*).

In the case presented here, we also had some problems assigning the periplasmic turns. In fact, only the first periplasmic turn which is like that of the wild type has been able to be assigned completely. The two other periplasmic turns which had to be extended by two and four residues for cloning purposes could not be assigned completely.

The specifically ^{15}N-labeled Leu sample (Figure 4) was used to verify the obtained assignment. We have to note that spectrum quality was a strong function of temperature, featuring a different appearance of resonances stemming from Leu situated in different positions in the protein scaffold. This experiment can be used to illustrate the major problem encountered in the process of resonance assignment of membrane proteins, namely, heterogeneity of the protein conformation on the time scale of chemical shifts, which appears to be a common feature of all studied membrane proteins.

Secondary Structure Identification of BBP+EF. The chemical shift index (CSI) analysis (Figure 5) and the identification of key interstrand ^{1}H^N−^{1}H^N NOEs clearly indicate the presence of eight β-strands. The CSI analysis was based on the C$^\alpha$ and C$^\beta$ chemical shifts of the assigned residues and the corresponding random coil shifts. As shown previously for soluble proteins, unbroken sequences of negative values of $\Delta C^\alpha - \Delta C^\beta$ indicate β-strand regions whereas positive values indicate α-helical regions (*57*). Thus far, however, there are not many cases in which ^{13}C chemical shifts have been used, directly or indirectly, to identify secondary structure elements for integral membrane proteins (*5*, *9*, *10*). For each pair of neighboring β-strands, a sufficient number of interstrand ^{1}H^N−^{1}H^N NOEs could be assigned in a 3D ^{15}N-resolved ^{1}H−^{1}H NOESY spectrum recorded on a 900 MHz spectrometer at 37 °C to establish the relative orientation of the β-strands (exemplified in Figure 6). The resulting relative orientation of β-strands agrees with the NMR structure of the TM domain of OmpA (*5*). BBP+EF adopts a meander topology; it is twisted to form an antiparallel closed eight-stranded β-barrel, in which the last β-strand is hydrogen bonded to the first. All strands are tilted relative to the membrane normal, and the shear number (*58*) of the β-barrel of BBP+EF is +10. The assignment of ^{1}H^N−^{1}H^N NOEs served as an independent verification of the sequence specific assignment determined earlier by analysis of the 3D ^{15}N−^{1}H TROSY-type triple-resonance experiments.

Collection of Conformational Restraints. Due to overall better quality and more homogeneous appearance of NMR spectra obtained with the BBP+EF construct, we decided to continue structural studies with only this protein. By comparing the chemical shifts of BBP and BBP+EF (data not shown), one can confidently assign all structural features of BBP+EF to BBP. For BBP+EF in total, only 27 characteristic interstrand ^{1}H^N−^{1}H^N NOEs have been able to be assigned (unambiguously), clearly demonstrating the need for other forms of structural constraints which do not rely on the NOE effect for integral membrane proteins with uniform side chain deuteration. Eleven additional interstrand and strand−loop NOEs could also be found. Of course, also

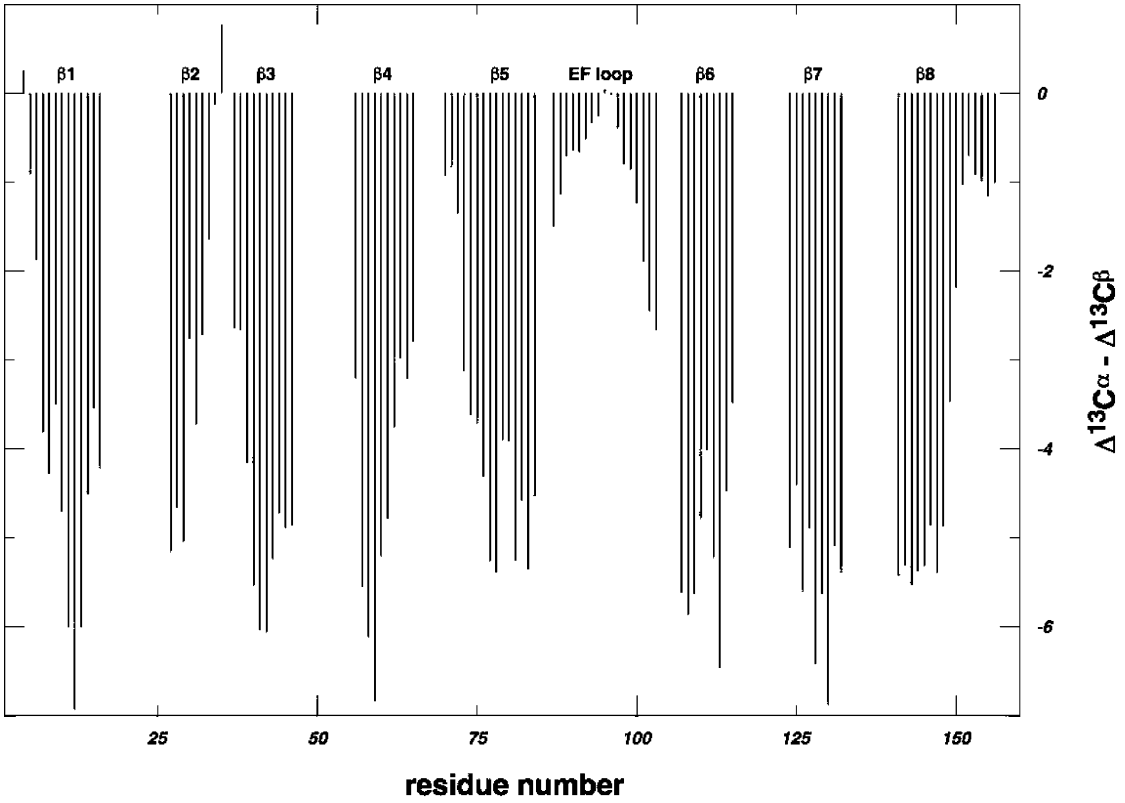

FIGURE 5: Plot of $\Delta^{13}C^{\alpha} - \Delta^{13}C^{\beta}$ vs the residue number. $\Delta^{13}C^{\alpha}$ and $\Delta^{13}C^{\beta}$ were obtained as the differences between the experimental $^{13}C^{\alpha}$ and $^{13}C^{\beta}$ chemical shifts of BBP+EF and the corresponding random coil shifts. The value of $\Delta^{13}C^{\alpha} - \Delta^{13}C^{\beta}$ used in the figure for any residue *i* is the arithmetic average over the three consecutive residues, $i - 1$, *i*, and $i + 1$. β-Strands $\beta1-\beta8$ are indicated at the top of each β-strand. The EF-hand loop inserted between $\beta5$ and $\beta6$ is also indicated. Regions with negative values of $\Delta^{13}C^{\alpha} - \Delta^{13}C^{\beta}$ indicate the presence of β-strands. Note that the numbering of the residues in this figure follows the BBP+EF sequence, not the sequence of the TM domain of OmpA.

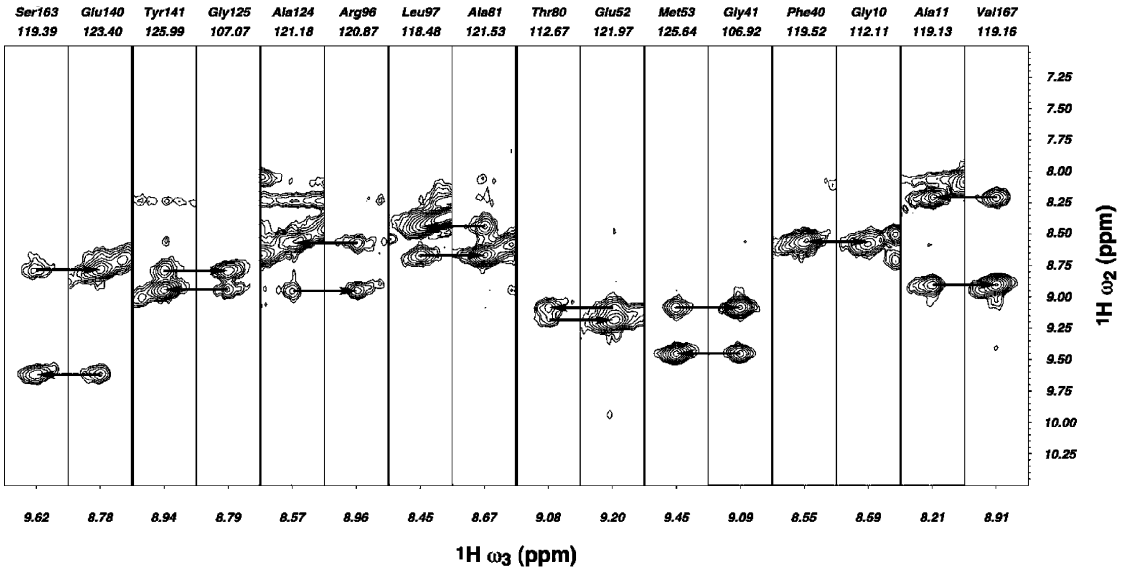

FIGURE 6: Strips from a 3D ^{15}N-resolved $^{1}H-^{1}H$ NOESY spectrum. The strips were extracted from the spectrum at the ^{15}N chemical shifts of each residue (indicated at the top of the each strip together with the sequence specific assignment). One pair of strips is shown for each pair of adjacent β-strands (the residues shown are colored purple in Figure 1B). Horizontal arrows point from long-range $^{1}H^{N}-^{1}H^{N}$ NOE cross-peaks (between β-strands) to intraresidual $^{1}H^{N}-^{1}H^{N}$ NOE cross-peaks. The spectrum was recorded at 900 MHz and 37 °C.

sequential $^{1}H^{N}-^{1}H^{N}$ NOEs were possible to identify. However, they do not significantly constrain the structure and were therefore only used as a consistency check of the assignment.

To obtain additional structural restraints, the $^{13}C^{\alpha}$, $^{13}C^{\beta}$, $^{13}C'$, and ^{15}N chemical shifts were analyzed with TALOS (*46*) to yield a collection of dihedral angle constraints. The TALOS calculations resulted in average ψ and ϕ angles and corresponding error ranges (typically 20−30°) for 62 residues.

To make comparisons against other β-barrel membrane protein structures (*5*, *9*, *10*) feasible and meaningful, 128 upper and 128 lower distance bounds corresponding to 64 hydrogen bonds (identified as in ref *5*) were used in the

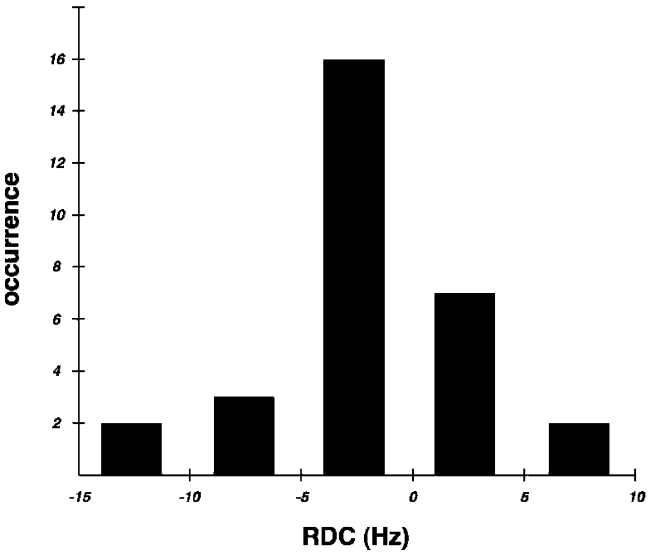

FIGURE 7: RDC distribution (from 27 couplings) for the BBP+EF+2G sample at 900 MHz and 37 °C. Alignment was achieved with 3 mM Tb^{3+}.

structure calculations.

From the limited number of long-range $^1H^N-^1H^N$ NOEs in this case, it is clear that constraints other than the classical NOE-derived distance constraints are essential for high-precision structure determination of integral membrane proteins with uniform side chain deuteration. This need for additional constraints is even more compelling for α-helical integral membrane proteins, since for these one cannot expect very many long-range $^1H^N-^1H^N$ NOEs. This is clearly illustrated by the four-helix bundle protein Mistic (*11*), for which site-directed spin-labels were utilized to produce distance-dependent line broadening perturbations that could be translated into distance constraints.

In this case, we chose the approach of obtaining additional constraints from RDCs. However, the titration of BBP+EF with Tb^{3+} ions gave only weak binding affinity with an estimated K_d of ~10 mM, which is not suitable for NMR studies. A significantly better affinity ($K_d \sim 1$ mM) for Tb^{3+} ions was observed for the insert containing two flanking Gly residues, BBP+EF+2G, which we used for our RDC measurements. The resulting affinity is still 2 orders of magnitude lower than that observed for the EF-hand loop in its native structural context. Several factors might contribute to the reduced affinity, such as a slightly different dynamically averaged geometry of the fusion points in BBP compared to calmodulin or the significant mobility of the structural context where we fused the loop. It is also very likely that the EF-hand loop does not have enough flexibility to fold into the conformation with the highest affinity for metal ions. For example, careful adjustment of the linker sequences between a host protein and an inserted loop was needed to optimize the metal bindning affinity of the engineered EF-hand loop into another scaffold protein (*23*). Due to the relatively low affinity of divalent cations of the La series, high concentrations of the paramagnetic ions are needed to induce a detectable degree of protein alignment even at 900 MHz of the static magnetic field. At this high concentration, nonspecific binding of metal ions to the protein results in uniform line broadening of many resonances, degrading the precision and number of RDCs amenable to structure refinement. This precludes the effective use of RDCs for statistically significant structure refinement in our case. However, the histogram of the measured RDCs (Figure 7) unequivocally demonstrates the alignment of the Tb^{3+}-loaded BBP+EF+2G at 900 MHz of the static magnetic field. Similar titrations with Tb^{3+} of BBP resulted in no detectable alignment of the protein (data not shown).

Global Fold Determination of BBP+EF. Structure calculations were performed with CYANA (*48*) (version 1.0). The input consisted of 38 NOE-derived upper distance limit constraints extracted from $^1H^N-^1H^N$ NOEs, 62 ψ and 62 ϕ dihedral angle constraints from $^{13}C^\alpha$, $^{13}C^\beta$, $^{13}C'$, and ^{15}N chemical shifts, and 128 upper distance limits and 128 lower distance limits corresponding to 64 hydrogen bonds. A total of 160 conformers were calculated by CYANA from random

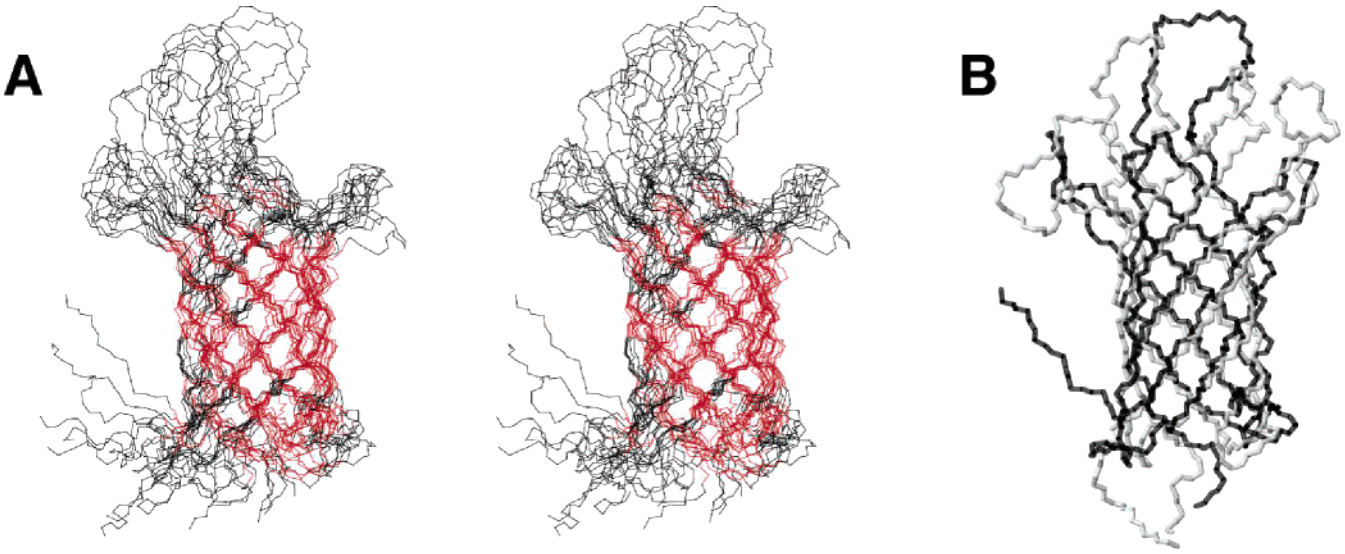

FIGURE 8: Structure of BBP+EF. (A) Stereo representation of the ensemble of 10 solution structures (with the lowest potential energy after the minimization by Gromacs) superimposed onto the average coordinates by minimizing the rmsds for the backbone atoms of β-strands. Only backbone atoms are shown. Residues subject to distance constraints originating from NOEs are colored red. (B) Ribbon representation of the BBP+EF structure with the lowest potential energy (black) and of the most representative OmpA (1G90) conformer (gray) with backbone atoms of β-barrel regions superimposed. Figures 8−10 were prepared with MOLMOL (*68*).

Table 1: Structural Statistics for BBP+EF

structural information	
no. of NOE distance constraints	38
no. of hydrogen bond constraints	128
no. of angle constraints	124
no. of NMR constraints violations[a]	
NOE	
sum (Å)	0.19 ± 0.09 (0.07−0.37)
maximum (Å)	0.06 ± 0.02 (0.02−0.09)
dihedral angle	
sum (deg)	2.48 ± 0.72 (1.45−3.75)
maximum (deg)	0.48 ± 0.21 (0.20−0.80)
rms deviation from corresponding mean structure (Å)	
all residues	
backbone atoms	3.21 ± 0.59
all heavy atoms	3.92 ± 0.49
residues in β-strands[b]	
backbone atoms	1.04 ± 0.24
all heavy atoms	1.98 ± 0.28
Ramachandran plot statistics (%)	
residues in allowed regions	96.2
residues in disallowed regions	3.8

[a] The values in parentheses are the observed ranges. [b] Assigned residues in the β-strands are 6−16, 27−34, 38−46, 56−65, 73−84, 106−115, 124−131, and 141−149.

starting structures. The 20 structures having the lowest CYANA target function values were selected and energy-minimized in vacuo, using Gromacs version 3.3.1 (*50*, *51*). Finally, the 10 structures with the lowest energy were selected to represent the NMR-derived global fold of BBP+EF in DHPC micelles (Table 1).

Figure 8A is a stereo representation of a superposition of the final 10 structures onto the corresponding average structure. The average root-mean-square deviation (rmsd) from the average coordinates is 1.0 Å for the backbone atoms when overlaying assigned residues in the eight β-strands. The structure is thus clearly of low precision as a result of the limited input data set, as seen by visual inspection of the ensemble of structures in Figure 8A. However, the backbone fold can readily be followed, and the achieved precision is sufficient to establish the similarities of the fold of BBP+EF and of the structure of the TM domain of OmpA (Figure 8B) determined by Tamm and co-workers (*5*). The precision of the loop regions is very low due to the lack of assignments and therefore also a lack of constraints. Although our calculated structures are not very precise, they exhibit backbone rmsds in the same range as the NMR structures of the TM domain of OmpA [1.2 Å (*5*)], OmpX [0.9 Å (*56*)], and PagP [0.8 and 0.9 for DPC and β-OG micelles, respectively (*10*)]. A Ramachandran plot reveals (data not shown) that 96.2% of the non-Gly residues have their ϕ and φ angles in allowed regions and 3.8% in disallowed regions. Ramachandran plots and the related statistics were generated using PROCHECK-NMR (*59*).

Backbone Dynamics of BBP+EF. To investigate the backbone dynamics of BBP+EF, we measured steady-state NOEs, which exhibit lower values for residues which are flexible on the nanosecond time scale. The values of the NOEs have been mapped onto the structure in Figure 9. The values of the NOEs are approximately 0.7 in the β-barrel and around 0.3 in the EF-hand loop. Clearly, the EF-hand loop is more mobile on the nanosecond time scale than the β-barrel. The average value of 0.7 for NOEs in the β-barrel

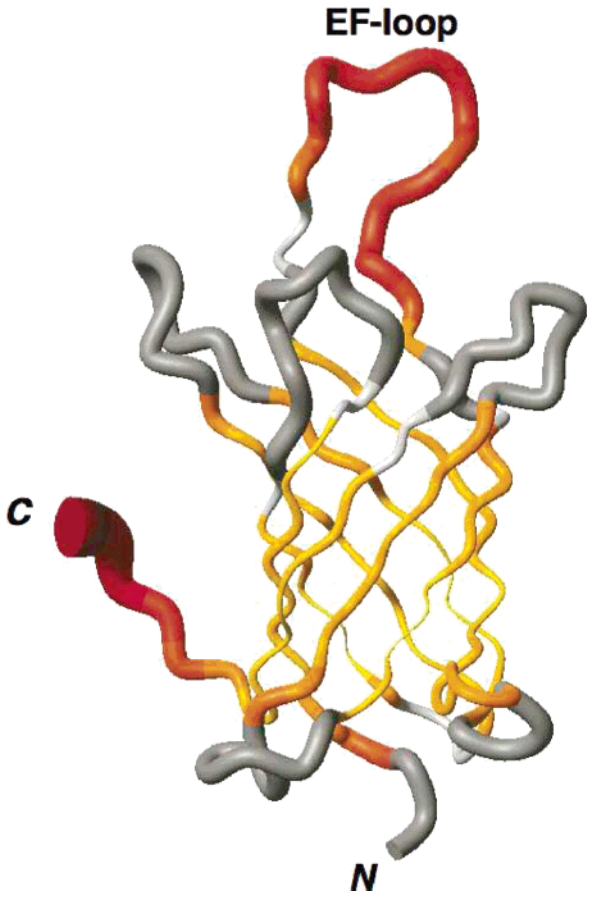

FIGURE 9: Tube representation of BBP+EF color-coded by the magnitude of the steady-state $^1H-^{15}N$ nuclear Overhauser effect (NOE). For residues with a maximal NOE (i.e., 1.0), the tube is thin and colored yellow. Correspondingly, for residues with smaller NOEs, the tube is thicker and increasingly red. For residues for which no value could be obtained due to overlap and there was no possibility to interpolate, the tube is colored light gray (in some cases, interpolation was possible and then the residue is color-coded accordingly). Finally, for residues for which sequence specific assignment has been impossible to achieve, the tube is colored dark gray. The EF-hand loop as well as the N- and C-termini are labeled.

of the TM domain of OmpA (*5*) is yet another indicator of strong similarities between BBP+EF and the TM domain of OmpA. The average value of NOEs for the loop regions of the TM domain of OmpA is 0.5; on the other hand, the EF-hand value is 0.3, indicating that the inserted EF-hand loop of BBP+EF is more mobile than the original loops of the TM domain of OmpA. The backbone dynamics of the TM domain OmpA are characterized by increasing gradients from the interior toward both ends of the β-barrel. The increased dynamics of the protein in both millisecond and nanosecond time scales in the region of both membrane surfaces may explain why the NMR signals of some residues in the highly mobile loops are broadened beyond detection. Similar trends (as for OmpA) in steady-state NOE values coupled with the increased line width of backbone resonances are seen for BBP+EF.

Calculating the average R_2/R_1 ratio for residues with negligible motions on the nanosecond time scale (NOE > 0.65 at 14.1 T, as is customary) after excluding residues with possible motions on the microsecond to millisecond time scale [according to the expression and criterion of Bax and co-workers (*13*)] gives a value of 120 ± 20 for BBP+EF.

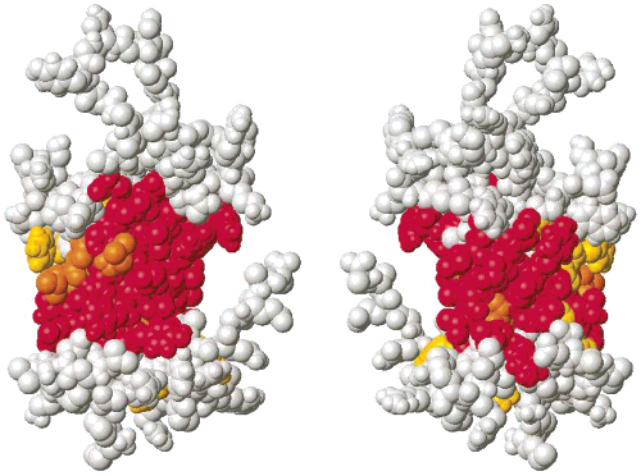

FIGURE 10: Space-filling all-atom representations of the surface of the NMR structure of BBP+EF in DHPC micelles. The residues that exhibited NOEs between the backbone amide proton and the hydrophobic tails of DHPC in a 3D ^{15}N-resolved ^{1}H−^{1}H NOESY spectrum are colored red. Residues for which no NOEs could be determined unambiguously due to overlap are colored orange if they are between two red-colored residues and yellow if they are preceding or succeeding a red-colored residue. Gray residues did not exhibit intermolecular NOEs to DHPC. The left and right views differ by a 180° rotation around the *y*-axis.

This yields an estimate of the single global rotational correlation time of 40 ± 6 ns according to relationship $J(\omega) = {}^{2}/_{5}S^{2}\tau_{c}/(1 + \omega^{2}\tau_{c}^{2})$ (with an assumption of isotropic molecular tumbling of micelle−protein complex and rigid protein scaffold with an S^2 of 0.9), indicating that the molecular mass of BBP+EF in DHPC micelles is on the order of 70−100 kDa.

BBP+EF−Detergent Interactions. Our studies of the interactions between BBP+EF and the detergent, DHPC, were based on the availability of the resonance assignments for DHPC (*60*). To determine the detergent-exposed surface of BBP+EF and to confirm the orientation of BBP+EF with respect to the membrane, we looked for NOEs between the amide protons of BBP+EF and the hydrophobic side chain protons of DHPC in a 3D ^{15}N-resolved ^{1}H−^{1}H NOESY spectrum recorded on a 600 MHz spectrometer at 37 °C. The residues that exhibit NOEs to the terminal methyl group (at 0.78 ppm) and to the penultimate and antepenultimate methylene (at 1.22 ppm) are mapped onto the surface of BBP+EF in Figure 10. A band of detergent interactions is apparent, as expected for an integral membrane protein.

Concluding Remarks. Our studies confirm previous results of Koebnik (*6*) indicating that the surface-exposed extracellular loops of the N-terminal TM domain of OmpA do not contain any folding topological determinants, since the protein construct lacking them folds into the well-defined β-barrel structure as described in this paper. Due to the ubiquitous use by Nature of the β-barrel folds, we might speculate that anchoring to the outer membrane or pore forming activity on the one side and external ligand binding functionality of extracellular elements on the other side might have evolved independently and, in fact, might constitute rather independent, noncorrelated functions. In the case of the TM domain of OmpA, these functions might be an anchoring of the periplasmatic polyglycan matrix to the outer membrane by the TM residues, pore forming activities and bacterial viral docking sites, and contribution to invasion of brain microvascular endothelial cells of the extracellular loops (*6*, *7*, *61*−*67*). Indirectly, this is confirmed by the successful engineering of a metal ion binding loop into the BBP scaffold. On the basis of this separation of functions, we suggest that BBP has the potential to be used as a template β-barrel membrane protein structure for the development of novel functions, although our results also highlight the potential difficulties that can arise when functionality is engineered into the loop regions of membrane proteins. Finally, the 142-residue BBP represents the smallest β-structured integral membrane protein known to date for which a 3D structure is available.

ACKNOWLEDGMENT

Prof. Dario Neri (Institute of Pharmaceutical Sciences, ETH Hönggerberg) is acknowledged for providing us with the plasmid containing the calmodulin gene of *X. laevis* and Prof. Volker Dötsch (University of Frankfurt, Frankfurt, Germany) is acknowledged for the transaminase knockout strain *E. coli* D39(DE3). We thank Dr. Rochus Keller for timely and high-quality support of his program CARA (http://www.nmr.ch).

REFERENCES

1. Koebnik, R., Locher, K. P., and Van Gelder, P. (2000) Structure and function of bacterial outer membrane proteins: Barrels in a nutshell, *Mol. Microbiol. 37*, 239−253.
2. Chen, R., Schmidmayr, W., Krämer, C., Chen-Schmeisser, U., and Henning, U. (1980) Primary structure of major outer membrane protein II (ompA protein) of *Escherichia coli* K-12, *Proc. Natl. Acad. Sci. U.S.A. 77*, 4592−4596.
3. Pautsch, A., and Schulz, G. E. (1998) Structure of the outer membrane protein A transmembrane domain, *Nat. Struct. Biol. 5*, 1013−1017.
4. Pautsch, A., and Schulz, G. E. (2000) High-resolution structure of the OmpA membrane domain, *J. Mol. Biol. 298*, 273−282.
5. Arora, A., Abildgaard, F., Bushweller, J., and Tamm, L. K. (2001) Structure of outer membrane protein A transmembrane domain by NMR spectroscopy, *Nat. Struct. Biol. 8*, 334−338.
6. Koebnik, R. (1999) Structural and functional roles of the surface-exposed loops of the β-barrel membrane protein OmpA from *Escherichia coli*, *J. Bacteriol. 181*, 3688−3694.
7. Ried, G., Koebnik, R., Hindennach, I., Mutschler, B., and Henning, U. (1994) Membrane topology and assembly of the outer membrane protein OmpA of *Escherichia coli* K12, *Mol. Gen. Genet. 243*, 127−135.
8. Popot, J. L., and Saraste, M. (1995) Engineering membrane proteins, *Curr. Opin. Biotechnol. 6*, 394−402.
9. Fernandez, C., Adeishvili, K., and Wüthrich, K. (2001) Transverse relaxation-optimized NMR spectroscopy with the outer membrane protein OmpX in dihexanoyl phosphatidylcholine micelles, *Proc. Natl. Acad. Sci. U.S.A. 98*, 2358−2363.
10. Hwang, P. M., Choy, W.-Y., Lo, E. I., Forman-Kay, J. D., Raetz, C. R. H., Privé, G. G., Bishop, R. E., and Kay, L. E. (2002) Solution structure and dynamics of the outer membrane enzyme PagP by NMR, *Proc. Natl. Acad. Sci. U.S.A. 99*, 13560−13565.
11. Roosild, T. P., Greenwald, J., Vega, M., Castronovo, S., Riek, R., and Choe, S. (2005) NMR structure of Mistic, a membrane-integrating protein for membrane protein expression, *Science 307*, 1317−1321.
12. Bax, A., and Grishaev, A. (2005) Weak alignment NMR: A hawk-eyed view of biomolecular structure, *Curr. Opin. Struct. Biol. 15*, 563−570.
13. Tjandra, N., Szabo, A., and Bax, A. (1996) Protein backbone dynamics and ^{15}N chemical shift anisotropy from quantitative measurement of relaxation interference effects, *J. Am. Chem. Soc. 118*, 6986−6991.
14. Clore, G. M., Starich, M. R., and Gronenborn, A. M. (1998) Measurement of residual dipolar couplings of macromolecules aligned in the nematic phase of a colloidal suspension of rod-shaped viruses, *J. Am. Chem. Soc. 120*, 10571−10572.

15. Hansen, M. R., Mueller, L., and Pardi, A. (1998) Tunable alignment of macromolecules by filamentous phage yields dipolar coupling interactions, *Nat. Struct. Biol. 5*, 1065−1074.
16. Koenig, B. W., Hu, J.-S., Ottiger, M., Bose, S., Hendler, R. W., and Bax, A. (1999) NMR measurement of dipolar couplings in proteins aligned by transient binding to purple membrane fragments, *J. Am. Chem. Soc. 121*, 1385−1386.
17. Sass, J., Cordier, F., Hoffmann, A., Rogowski, M., Cousin, A., Omichinski, J. G., Löwen, H., and Grzesiek, S. (1999) Purple membrane induced alignment of biological macromolecules in the magnetic field, *J. Am. Chem. Soc. 121*, 2047−2055.
18. Burns, P. D., and LaMar, G. N. (1982) Proton spin relaxation for the nonlabile coordinated chelate in lanthanide shift reagents, *J. Magn. Reson. 46*, 61−68.
19. Veglia, G., and Opella, S. J. (2000) Lanthanide ion binding to adventitious sites aligns membrane proteins in micelles for solution NMR spectroscopy, *J. Am. Chem. Soc. 122*, 11733−11734.
20. Ma, C., and Opella, S. J. (2000) Lanthanide ions bind specifically to an added "EF-hand" and orient a membrane protein in micelles for solution NMR spectroscopy, *J. Magn. Reson. 146*, 318−384.
21. Howell, S. C., Mesleh, M. F., and Opella, S. J. (2005) NMR structure determination of a membrane protein with two transmembrane helices in micelles: MerF of the bacterial mercury detoxification system, *Biochemistry 44*, 5196−5206.
22. Cierpicki, T., Liang, B., Tamm, L. K., and Bushweller, J. H. (2006) Increasing the accuracy of solution NMR structures of membrane proteins by application of residual dipolar couplings. High-resolution structure of outer membrane protein A, *J. Am. Chem. Soc. 128*, 6947−6951.
23. Ye, Y., Lee, H.-W., Yang, W., Shealy, S. J., Wilkins, A. L., Liu, Z.-R., Torshin, I., Harrison, R., Wohlhueter, R., and Yang, J. J. (2001) Metal binding affinity and structural properties of an isolated EF-loop in a scaffold protein, *Protein Eng. 14*, 1001−1013.
24. Ye, Y., Shealy, S., Lee, H.-W., Torshin, I., Harrison, R., and Yang, J. J. (2003) A grafting approach to obtain site-specific metal-binding properties of EF-hand proteins, *Protein Eng. 16*, 429−434.
25. Linse, S., Helmersson, A., and Forsen, S. (1991) Calcium binding to calmodulin and its globular domains, *J. Biol. Chem. 266*, 8050−8054.
26. Bertini, I., Gelis, I., Katsaros, N., Luchinat, C., and Provenzani, A. (2003) Tuning the affinity for lanthanides of calcium binding proteins, *Biochemistry 42*, 8011−8021.
27. Ye, Y., Lee, H.-W., Yang, W., and Yang, J. J. (2005) Calcium and lanthanide affinity of the EF-loops from the C-terminal domain of calmodulin, *J. Inorg. Biochem. 99*, 1376−1383.
28. Fiaux, J., Bertelsen, E. B., Horwich, A. L., and Wüthrich, K. (2004) Uniform and residue-specific ^{15}N-labeling of proteins on a highly deuterated background, *J. Biomol. NMR 29*, 289−297.
29. Box, G. E. P., Hunter, W. G., and Hunter, J. S. (1978) *Statistics for Experimenters*, John Wiley & Sons, New York.
30. Chen, G.-Q., and Gouaux, E. (1997) Overexpression of a glutamate receptor (GluR2) ligand binding domain in *Escherichia coli*: Application of a novel protein folding screen, *Proc. Natl. Acad. Sci. U.S.A. 94*, 13431−13436.
31. Armstrong, N., de Lencastre, A., and Gouaux, E. (1999) A new protein folding screen: Application to the ligand binding domains of a glutamate and kainate receptor and to lysozyme and carbonic anhydrase, *Protein Sci. 8*, 1475−1483.
32. Expert-Bezancon, N., Rabilloud, T., Vuillard, L., and Goldberg, M. E. (2003) Physical-chemical features of non-detergent sulfobetaines active as protein-folding helpers, *Biophys. Chem. 100*, 469−479.
33. Burns, R. A., Roberts, M. F., Dluhy, R., and Mendelsohn, R. (1982) Monomer-to-micelle transition of dihexanoylphosphatidylcholine: ^{13}C NMR and Raman studies, *J. Am. Chem. Soc. 104*, 430−438.
34. Pervushin, K., Riek, R., Wider, G., and Wüthrich, K. (1997) Attenuated T_2 relaxation by mutual cancellation of dipole-dipole coupling and chemical shift anisotropy indicates an avenue to NMR structures of very large biological macromolecules in solution, *Proc. Natl. Acad. Sci. U.S.A. 94*, 12366−12371.
35. Salzmann, M., Pervushin, K., Wider, G., Senn, H., and Wüthrich, K. (1998) TROSY in triple-resonance experiments: New perspectives for sequential NMR assignments of large proteins, *Proc. Natl. Acad. Sci. U.S.A. 95*, 13585−13590.
36. Salzmann, M., Wider, G., Pervushin, K., Senn, H., and Wüthrich, K. (1999) TROSY-type triple-resonance experiments for sequential NMR assignmnets of large proteins, *J. Am. Chem. Soc. 121*, 844−848.
37. Talluri, S., and Wagner, G. (1996) An optimized 3D NOESY-HSQC, *J. Magn. Reson., Ser. B 112*, 200−205.
38. Zhu, G., Xia, Y., Nicholson, L. K., and Sze, K. H. (2000) Protein dynamics measurements by TROSY-based NMR experiments, *J. Magn. Reson. 143*, 423−426.
39. Pervushin, K. V., Wider, G., and Wüthrich, K. (1998) Single transition-to-single transition polarization transfer (ST2-PT) in [^{15}N,^{1}H]-TROSY, *J. Biomol. NMR 12*, 345−348.
40. Güntert, P., Dötsch, V., Wider, G., and Wüthrich, K. (1992) Processing of multi-dimensional NMR data with the new software PROSA, *J. Biomol. NMR 2*, 619−629.
41. Keller, R. L. J. (2004) *The computer aided resonance assignment tutorial*, 1st ed., CANTINA Verlag, Goldau.
42. Keller, R. L. J. (2004) Optimizing the process of nuclear magnetic resonance analysis and computer aided resonance assignment, Ph.D. Dissertation, ETH Hönggerberg, Zurich.
43. Markley, J. L., Bax, A., Arata, Y., Hilbers, C. W., Kaptein, R., Sykes, B. D., Wright, P. E., and Wüthrich, K. (1998) Recommendations for the presentation of NMR structures of proteins and nucleic acids, *J. Biomol. NMR 12*, 1−23.
44. Wishart, D. S., Bigam, C. G., Yao, J., Abildgaard, F., Dyson, H. J., Oldfield, E., Markley, J. L., and Sykes, B. D. (1995) ^{1}H, ^{13}C and ^{15}N chemical shift referencing in biomolecular NMR, *J. Biomol. NMR 6*, 135−140.
45. Wüthrich, K. (1986) *NMR of Proteins and Nucleic Acids*, John Wiley & Sons, New York.
46. Cornilescu, G., Delaglio, F., and Bax, A. (1999) Protein backbone angle restraints from searching a database for chemical shift and sequence homology, *J. Biomol. NMR 13*, 289−302.
47. Gardner, K. H., Rosen, M. K., and Kay, L. E. (1997) Global folds of highly deuterated, methyl-protonated proteins by multidimensional NMR, *Biochemistry 36*, 1389−1401.
48. Güntert, P., Mumenthaler, C., and Wüthrich, K. (1997) Torsion angle dynamics for NMR structure calculation with the new program DYANA, *J. Mol. Biol. 273*, 283−298.
49. Polak, E., and Ribière, G. (1969) Note sur la convergence de méthodes de directions conjugées, *Rev. Fr. Informatique Recherche Opérationelle 16*, 35−43.
50. Berendsen, H. J. C., van der Spoel, D., and van Drunen, R. (1995) GROMACS: A message-passing parallel molecular dynamics implementation, *Comput. Phys. Commun. 91*, 43−56.
51. Lindahl, E., Hess, B., and van der Spoel, D. (2001) Gromacs 3.0: A package for molecular simulation and trajectory analysis, *J. Mol. Model. 7*, 306−317.
52. van Gunsteren, W. F., Billeter, S. R., Eising, A. A., Hünenberger, P. H., Krüger, P., Mark, A. E., Scott, W. R. P., and Tironi, I. G. (1996) *Biomolecular Simulation: The GROMOS96 manual and user guide*, Hochschulverlag AG an der ETH Zurich, Zurich.
53. Pautsch, A., Vogt, J., Model, K., Siebold, C., and Schulz, G. E. (1999) Strategy for membrane protein crystallization exemplified with OmpA and OmpX, *Proteins 34*, 167−172.
54. Koebnik, R. (1996) In vivo membrane assembly of split variants of the *E. coli* outer membrane protein OmpA, *EMBO J. 15*, 3529−3537.
55. Koebnik, R., and Kramer, L. (1995) Membrane assembly of circularly permuted variants of the *E. coli* outer membrane protein OmpA, *J. Mol. Biol. 250*, 617−626.
56. Fernandez, C., Hilty, C., Bonjour, S., Adeishvili, K., Pervushin, K., and Wüthrich, K. (2001) Solution NMR studies of the integral membrane proteins OmpX and OmpA from *Escherichia coli*, *FEBS Lett. 504*, 173−178.
57. Wishart, D. S., and Sykes, B. D. (1994) The ^{13}C Chemical-Shift-Index: A simple method for the identification of protein secondary structure using ^{13}C chemical-shift data, *J. Biomol. NMR 4*, 171−180.
58. McLachlan, A. D. (1979) Gene duplications in the structural evolution of chymotrypsin, *J. Mol. Biol. 128*, 49−79.
59. Laskowski, R. A., Rullmann, J. A. C., MacArthur, M. W., Kaptein, R., and Thornton, J. M. (1996) AQUA and PROCHECK-NMR: Programs for checking the quality of protein structures solved by NMR, *J. Biomol. NMR 8*, 477−486.
60. Fernandez, C., Hilty, C., Wider, G., and Wüthrich, K. (2002) Lipid-protein interactions in DHPC micelles containing the integral membrane protein OmpX investigated by NMR spectroscopy, *Proc. Natl. Acad. Sci. U.S.A. 99*, 13533−13537.

61. Sugawara, E., and Nikaido, H. (1992) Pore-forming activity of OmpA protein of *Escherichia coli*, *J. Biol. Chem. 267*, 2507−2511.
62. Saint, N., De, E., Julien, S., Orange, N., and Molle, G. (1993) Ionophore properties of OmpA of *Escherichia coli*, *Biochim. Biophys. Acta 1145*, 119−123.
63. Sugawara, E., and Nikaido, H. (1994) OmpA protein of *Escherichia coli* outer membrane occurs in open and closed channel forms, *J. Biol. Chem. 269*, 17981−17987.
64. Rodionova, N. A., Tatulian, S. A., Surrey, T., Jahnig, F., and Tamm, L. K. (1995) Characterization of two membrane-bound forms of OmpA, *Biochemistry 34*, 1921−1929.
65. Prasadarao, N. V., Wass, C. A., Weiser, J. N., Stins, M. F., Huang, S. H., and Kim, K. S. (1996) Outer membrane protein A of *Escherichia coli* contributes to invasion of brain microvascular endothelial cells, *Infect. Immun. 64*, 146−153.
66. Klesney-Tait, J., Hiltke, T. J., Maciver, I., Spinola, S. M., Radolf, J. D., and Hansen, E. J. (1997) The major outer membrane protein of *Haemophilus ducreyi* consists of two OmpA homologs, *J. Bacteriol. 179*, 1764−1773.
67. Buchanan, S. K. (1999) β-Barrel proteins from bacterial outer membranes: Structure, function and refolding, *Curr. Opin. Struct. Biol. 9*, 455−461.
68. Koradi, R., Billeter, M., and Wüthrich, K. (1996) MOLMOL: A program for display and analysis of macromolecular structures, *J. Mol. Graphics 14*, 51−55.

BI061265E